

This is the author's accepted manuscript of the following article:

Hubel, T. Y., Hristov, N. I., Swartz, S. M. and Breuer, K. S. (2016) 'Wake structure and kinematics in two insectivorous bats', *Philosophical Transactions of the Royal Society B: Biological Sciences*, 371(1704).

The final publication is available at Royal Society via <https://doi.org/10.1098/rstb.2015.0385>.

The full details of the published version of the article are as follows:

TITLE: Wake structure and kinematics in two insectivorous bats

AUTHORS: Hubel, T. Y., Hristov, N. I., Swartz, S. M. and Breuer, K. S.

JOURNAL TITLE: Philosophical Transactions of the Royal Society B: Biological Sciences

PUBLICATION DATE: September 2016

PUBLISHER: Royal Society

DOI: 10.1098/rstb.2015.0385

Wake structure and kinematics in two insectivorous bats

Tatjana Y. Hubel^{1,2}, Nickolay I. Hristov^{3,4}, Sharon M. Swartz^{1,3}, Kenneth S. Breuer^{1,3}

¹*School of Engineering, and* ³*Department of Ecology and Evolutionary Biology, Brown University, Providence, RI 02912, USA*

²*Structure and Motion Laboratory, Royal Veterinary College, Hatfield AL97TA, UK*

⁴*Center for Design Innovation, Winston Salem, NC 27101-4019, USA*

Keywords: bat flight, wake structure, flapping flight

ABSTRACT

We compare kinematics and wake structure over a range of flight speeds (4.0-8.2 ms⁻¹) for two bats that pursue insect prey aerially, *Tadarida brasiliensis* and *Myotis velifer*. Body mass and wingspan are similar in these species, but *M. velifer* has broader wings and lower wing loading. By using high speed videography and particle image velocimetry of steady flight in a wind tunnel, we show that 3D kinematics and wake structure are similar in the two species at the higher speeds studied, but differ at lower speeds. At lower speeds, the two species show significant differences in mean angle of attack, body-wingtip distance and sweep angle. The distinct body vortex seen at low speed in *T. brasiliensis* and other bats studied to date is considerably weaker or absent in *M. velifer*. We suggest that this could be influenced by morphology: 1) the narrower thorax in this species likely reduces the body-induced discontinuity in circulation between the two wings; and 2) the wing loading is lower, hence the lift coefficient required for weight support is lower. As a result, in *M. velifer*, there may be a decreased disruption in the lift generation between the body and the wing and the strength of the characteristic root vortex is greatly diminished, both suggesting increased flight efficiency.

INTRODUCTION

To fly, animals face a host of physical and biological challenges. The rich diversity of extant flapping flyers encompasses many variations on basic themes, whether one considers aerodynamic force production, control of trajectories in three-dimensional aerial environments, or how flight is employed to obtain food, escape predation or injury, and to reproduce. As the comparative biology of animal flight continues to mature, it has been possible to discern important commonalities in how flying animals interact with the physical world. For example, insects, bats, and birds cruise at similar Strouhal numbers ($St = \text{frequency} \times \text{amplitude} / \text{speed}$; predictor of the unsteadiness of the flow over the wing) [1]; passive rotational damping plays a key role in turning dynamics for all flying animals studied to date [2]; and for some modes of flight, high lift is generated by a stable leading edge vortex in multiple kinds of animals [3-7].

Within these basic similarities, however, distinct differences occur among flying animals at many levels of organization. Body size profoundly influences multiple aspects of flight, from fluid dynamics to muscle physiology to wing loading. Hence flight is experienced quite differently by insects with wings less than one mm in length (e.g. [8]) compared to large migratory birds or raptors (e.g. [9, 10]). Because the four known evolutionary origins of flight are phylogenetically distant, the basic anatomy and material composition of the flight apparatus are fundamentally different in insects, pterosaurs, birds, and bats. Major differences in the mechanical properties of wing tissues can be observed among groups of flying animals (see, for example, [11-15]), and these have significant consequences for flight function. Details of patterns of wing motion, too, differ between insects, birds, and bats. At a finer taxonomic scale, within each of the major lineages of flying animals, wingbeat kinematics can vary substantially among species (e.g. [16-18]). Similarly, some aspects of wake architecture may be characteristic of insects, birds, or bats (see [7]), but there is variation within each group that appears to be associated with kinematics, wing morphology or both (insects: hawkmoths[19] vs locusts[19, 20]; birds: blackcaps[21] vs. swifts[22]; bats: Pallas' long-tonged bats[23] vs Brazilian free-tailed bats [24]).

Morphology, kinematics and flight performance are interrelated, and may be associated with diverse aspects of a given species' ecology [25]. However, although correlations between wing geometry and ecology have been sought for several decades (e.g. [25-29]), the power of detailed fluid dynamics analysis to improve understanding of functional differences between species whose flight apparatus shares many similarities has yet to be fully realized (but see [20, 30]).

The choice of study species that exemplify particular traits, from lineages of known phylogenetic relatedness, can provide new insight into associations among wing structure, aerodynamics, and flight capabilities. To date, all but one of the bat species whose wakes have been studied in detail have been similar in feeding ecology (fruit- and nectar-feeding) and were drawn from two rather distantly related families, the Pteropodidae and Phyllostomidae [23, 31-34]. Species of these two families generally have short wings and relatively high wing loading [25, 35] and have similar wake structure over the wingbeat cycle. In contrast, the molossid *Tadarida brasiliensis*, the Brazilian free-tailed bat, differs from frugivores and nectarivores in flight ecology, wing kinematics, morphology, and wake dynamics [24, 25]. This aerial hunter resembles the common swift (*Apus apus*) in wing form and wake architecture [24, 36]. This suggests that in both birds and bats, ecology, flight performance, morphology and aerodynamics can show common patterns of interrelationship, despite fundamental differences in the structure of the flight apparatus in these distantly related flying vertebrates [24].

Here we explore whether there are differences in kinematics and wake structure between two bat species whose ecology is broadly similar but differs in notable ways on a finer scale. For this comparison, we chose species from distantly related families: *Myotis velifer* (Vespertilionidae) and *Tadarida brasiliensis* (Molossidae), who last shared a common ancestor more than 50 million years ago [37]. The two species often share roost sites, are comparable in weight and wingspan and are aerial insectivores, catching their prey on the wing.

T. brasiliensis is known for its migration and ability to commute long distances for feeding [38-40]. It forages in open spaces high above the ground with fast straight flight [41, 42]. Bats of this species possess relatively high wing loading and aspect ratio, as well as pointed wing tips, and it has been proposed that these traits could be

associated with great agility (rate at which turns can be initiated) and high efficiency when flying at higher speeds [25, 43, 44]. However, this wing shape requires higher flight speeds to generate sufficient lift to support body weight, suggesting they may also possess lower maneuverability (turning radius at given speed) and poorer performance at lower speeds [25]. In contrast, *M. velifer* does not migrate, and instead hibernates in winter. This species hunts closer to the ground, where it likely encounters more obstacles, such as vegetation and rock formations [45]. It has been reported that the flight of *M. velifer* is more direct, with less flutter, than that of other species of the genus [39], but not as straight as *T. brasiliensis*. *M. velifer* shows a slightly higher aspect ratio than average, though still lower than *T. brasiliensis* [46]. *M. velifer*'s low wing loading, relatively long wings and round wing tips are hypothesized to be associated with slow, economic and maneuverable flight [25, 43, 47].

In this study we compare the kinematics and wake architecture of *M. velifer* and *T. brasiliensis*, and hypothesise that these will reflect differences in wing shape and ecology of these two species. We also explored flight speed-dependence of the differences between the species. Due to their ecology, we expected that the migratory *T. brasiliensis* might be more tuned towards fast flight, while *M. velifer* would favour slightly lower speeds. We discuss our findings in the context of similar studies on bats with different ecology and morphology (fruit- and nectar-feeding) and birds with similar aerial foraging strategies.

MATERIALS AND METHODS

We used particle image velocimetry (PIV) and high speed videography to investigate the wake structure of two bat species, *M. velifer* and *T. brasiliensis*. Wake structure and kinematics for *T. brasiliensis* have previously been published [24].

Bats

We compared wake structure in *M. velifer* (three female and one male) to that of *T. brasiliensis* (two females and three males). All bats were wild-caught at the same cave in Texas in April 2009.

Morphological descriptors of each individual were extracted from high speed video of flights at low speed (all trials $< 5.5 \text{ ms}^{-1}$) using the direct linear transformation (DLT) method[48] for 3D reconstruction.

We selected the point of the wingbeat cycle at which wing extension was greatest, typically close to the middle of the downstroke. Half wingspan (\mathbf{b}) was defined as the maximum distance between the point midway between the scapulae and the wingtip at mid-downstroke, and wing chord (\mathbf{c}) as the maximum distance between wrist and the tip of the fifth digit (Fig. 1). Wing area (\mathbf{S}) was the area enclosed by markers at the midline point between the scapulae, wrist, wingtip, tip of the digit V, and foot. To assess the effect of estimating area by five points instead of the wing outline, we compared area estimated by these two alternatives from dorsal views of low speed flights (one per bat, Fig. 2). Images were selected at maximum wing extension during the downstroke and processed using Adobe Illustrator (Adobe, San Jose, CA). Wing area estimated from a full outline was 1.4% smaller compared to the five point-estimate for *T. brasiliensis* and 0.7% for *M. velifer*. We deemed this difference insubstantial relative to the additional data processing required to compute wing area by the full outline method.

We computed aspect ratio (\mathbf{AR}) as $2*(\mathbf{b}^2/\mathbf{S})$, and wing loading (\mathbf{Q}) as $0.5*mg/\mathbf{S}$. Tail area and width of the trunk were extracted from the dorsal view of one trial per individual at low speed (Fig. 2). We calculated means and standard deviations for each bat for chord, half wingspan, body mass, wing area, aspect ratio, and wing loading from all complete wingbeat cycles in trials at speeds between 4.0 ms^{-1} and 5.5 ms^{-1} (Table 1). Values for morphological parameters such as wingspan and chord measured in this manner in flight can differ from those measured on bats placed in a maximally flattened posture with wing joints maximally extended, but are more directly relevant for specific flight conditions under study [49].

Experimental setup

Bats were trained to fly over a range of speeds ($4.0\text{-}8.2 \text{ ms}^{-1}$) in the wind tunnel at Brown University (test section 0.60 by 0.82 by 3.8 m height x width x length)[24]. Synchronized PIV and high speed video recordings were carried out for all study subjects. The illumination plane of the PIV laser (Litron LPY 703-200, 200 Hz) was oriented perpendicular to the free stream and particles of DEHS (di-ethyl-hexyl-sebacate) were used for seeding. Two PIV cameras (Photron 1024 PCI, 1024×1024

pixel, lens 85 mm, f/1.4) were positioned downstream from the bats in the test section, stacked vertically to capture slightly overlapping images, yielding a composite image with final size of 0.25 m x 0.45 m (width x height). Kinematics were recorded by three high-speed video cameras (Photron 1024 PCI, 200Hz, shutter speed 1/1000 s) positioned outside the wind tunnel. 3-D kinematics were reconstructed from five anatomical markers: dorsal midline (between scapulae), wrist, tip of 3rd and 5th digits, and foot (Fig. 1a), using the DLT method. PIV and kinematics were sampled at 200 Hz, producing approximately 25-40 recordings per wingbeat.

Although stationary feeders can be used to train nectar-feeding bats to fly at a given position in a wind tunnel, this approach is not appropriate to insectivorous bats. Instead, the bats flew upstream through the test section somewhat faster than the free stream velocity, although far more slowly than in the presence of no wind. They subsequently landed on a mesh screen after they passed through the measurement volume. The bat was released in front of the PIV cameras and recording was triggered manually after the bat passed the position of the laser sheet. Net or total flight speed (U_t) was the sum of wind tunnel and forward flight speeds. The synchronization between kinematic and PIV measurements required correction of the “Doppler shift” in the time-resolved PIV fields due to the additional speed of the bats flying towards the front of the wind tunnel [32].

Trials were saved for analysis only when the bat flew straight and level in the middle of the wind tunnel test section, and within the limited observation area of the PIV system. Approximately one in five trials were usable. Bats flew up to 15 times in one session, and individuals rested at least one day between sessions. Flights were rewarded with a mealworm. The bat’s weight was measured before the first flight and adjusted by the weight of the mealworms consumed over the course of the experiment. We collected an average of 20 usable trials per individual for *T. brasiliensis* and about 9 usable trials per individual for *M. velifer*. Both species flew over range of speeds with *M. velifer* covering speeds between 3.8 and 8.2 ms⁻¹ and *T. brasiliensis* covering speeds between 4.0 and 9.3 ms⁻¹. We only compared overlapping speeds from 4.0 ms⁻¹ to 8.2 ms⁻¹, removing one trial below 4.0 ms⁻¹ from *M. velifer* and 10 trials above 8.2 ms⁻¹ from the original *T. brasiliensis* dataset [24].

PIV analysis software, DaVis v. 7.2 (LaVision Inc., Ypsilanti, MI, USA) was used to generate the velocity vector fields by applying sequential cross-correlation with multi-pass iterations in decreasing size (128x128 pixel, 2 iterations to 64x64 pixel, 2 iterations, 50% overlap). Vectors with a peak ratio Q of < 1.2 and an average neighbourhood variation of $> 1.5 \times \text{rms}$ were replaced by post-processing interpolation and the application of a simple 3×3 smoothing filter. Vector fields were then exported and further processing was conducted in MATLAB (Mathworks Inc., Natick, MA, USA).

Vorticity and swirl were computed to visualize wake structures [24, 33, 50]. Vector fields and vorticity were displayed using a $\pm 5 \text{ s}^{-1}$ vorticity threshold ($< 5\%$ of maximum vorticity value in trial) to reduce noise. Swirl is closely related to velocity, but distinguishes between shear and rotation [50]. By using positive swirl values, thus only displaying rotational information, noise is greatly reduced in the isosurface reconstructions. Vorticity was smoothed using a 3×3 smoothing filter, swirl was calculated, and a threshold of 25 ($< 1\%$ of maximum swirl value in trial) was applied to eliminate remaining noise. The rotational direction and circulation was determined from vorticity.

Four vortices have been identified in the typical wake of bats [33, 51]: a wingtip vortex, a wing root vortex and a distal wing vortex pair. The circulation for each vortex, over the course of the wingbeat cycle, was calculated by identifying the vortex location manually and integrating vorticity over the surrounding adjacent area after applying a 5 s^{-1} threshold.

Results are presented in a body-centred coordinate system, or a combination of global- and body-centred systems. Both reference frames are based on right-handed coordinate systems with positive x in wind direction, positive z in vertical or upward direction, and positive y in the direction of the right wingtip from the centre of the bat's body. The origin of the bat-centred system is the mid-body marker, and the global coordinate system originates at the position of the laser light sheet.

Kinematics were analysed by interpolating information to 40 time points per wingbeat cycle, starting at the upper reversal point of the wingtip. Two surface planes were defined to characterize 3D wing orientation (Fig. 1a): the armwing, defined by wrist, sternum and 5th digit, and handwing, defined by wrist, digit V and wing tip. The following parameters were calculated (Fig. 1):

Flapping frequency, f , wingbeats per second

Downstroke ratio, τ , downstroke period/total wingbeat period, defined by vertical wingtip motion

Wing stroke amplitude, Θ_{tip} , maximum angle of excursion of shoulder to wingtip over the wingbeat cycle

Span ratio, SR , ratio of upstroke to downstroke wingspan when the wing passed through the horizontal plane (Fig. 1b)

Stroke plane angle, β , angle between a line connecting the wingtip at the upper and lower reversal point in the side view (xz plane) relative to the horizontal

Angle of attack, α , the angle between the armwing surface and the effective air velocity, the vector sum of net bat speed (U_t), and wing velocity (Fig. 1c) (α_{md} is at mid-downstroke and α_{mean} is the average α over the wingbeat cycle)

Wrist sweep angle, ϕ , rotation of the handwing relative to the armwing, along the axis defined by wrist and the fifth digit (decrease in ϕ is a backwards sweeping motion)

Wrist flexion angle, θ , rotation of the handwing in the axis perpendicular to the armwing (angle above 180° corresponds to downward flexion)

Analysis

We analysed no more than three wing beat cycles per trial, for a total of 215 wing beat cycles (99 trials) for *T. brasiliensis* and 70 wing beat cycles (35 trials) for *M. velifer*. A significance level of 5% was used for all tests, which were performed using SPSS 17.0 (SPSS Inc., Chicago, IL, USA).

Bats flew at a range of speeds not strictly defined by wind tunnel airspeed due to their movement upstream. We first explored the relationship between flight parameters and speed for each species separately, treating speed as a continuous variable (Suppl. Table 1, [24]). We employed a mixed-effect model with reduced maximum likelihood

estimates of the variance (REML). Wingbeat cycle was treated as a repeated measure and individual as a random effect. To counteract the problem of multiple comparisons, p -values were corrected using the sequential Holm-Bonferroni method (p' -values). We then explored the data further by comparing species, as well as allowing for polynomial functions of second and third order in case of a non-linear relationship between parameter and speed [52]. Best fit was determined based on log-likelihood ratio (-2LL) (Fig. 3).

To visualize differences in dynamics and kinematics in relation to speed and to facilitate comparison between the two species (Table 2), we grouped trials into three net flight speed categories: low, 4.0 to 5.5 ms^{-1} ; medium, 5.5 ms^{-1} to 7 ms^{-1} and high, 7 ms^{-1} to 8.2 ms^{-1} . Because *M. velifer* and *T. brasiliensis* differ little in body mass, we did not normalize the data by flight speed or wing chord. Wing chord-normalised kinematics are presented in supplementary material (Suppl. Fig. 1). A mixed-effect model with individual as random effect, wingbeat cycle as repeated measure, species as fixed effect, and Holm-Bonferroni correction, was used to compare kinematic parameters among the speed groups. To compare wing trajectories and circulation among groups graphically, we first computed averages of the respective variables for all wingbeat cycles within a trial, then averaged all trials for each bat before computing averages for all bats (see Fig. 4,6). Standard errors are calculated over individuals.

RESULTS

Kinematics

Those flight parameters that change significantly with flight speed change less in *M. velifer* than *T. brasiliensis* (Fig. 3). In addition, the two species differ substantially more in their kinematics at low speed (Fig. 3).

Although variation in flight parameters with flight speed is subtle, several parameters change significantly in *M. velifer* (Suppl. Table 1, speed treated as continuous variable). Maximum half wingspan ($p'=0.020$), minimum body-wingtip distance ($p'=0.040$), and mean angle of attack ($p'=0.027$) decrease with increasing flight

speed, while wingbeat amplitude increases ($p' < 0.001$). Frequency ($p' = 0.098$), span ratio ($p' = 0.895$), downstroke angle of attack ($p' = 1.000$), sweep ($p' = 1.000$) and flexion ($p' = 1.000$) angles, downstroke ratio ($p' = 0.895$), stroke plane angle ($p' = 0.678$), wing chord ($p' = 1.000$) do not change significantly with flight speed. In contrast, in *T. brasiliensis*, all kinematic parameters except stroke plane angle ($p' = 0.956$) and maximum wing chord ($p' = 0.956$) change significantly with speed. Frequency ($p' = 0.001$), downstroke ratio ($p' = 0.004$), span ratio ($p' = 0.004$), maximum span ($p' = 0.005$), minimum body-wingtip distance ($p' = 0.005$), downstroke angle of attack ($p' = 0.005$), mean angle of attack ($p' = 0.005$), sweep angle ($p' = 0.005$) and flexion angle ($p' = 0.005$) all decreased, while wingbeat amplitude ($p' = 0.002$) was the only parameter that increased significantly (Suppl. Table 1, [24]).

Closer examination of the differences between flight speeds as well as between species were achieved separating kinematics into three flight speed categories. Wing position trajectories confirm that the large-scale spatial geometry of wingbeat kinematics changes little with speed at the velocities we assessed in *M. velifer* (Fig. 4a-f,g,i,k, Suppl. Table 1, Table 2). We observed a small shift in absolute position of wingtip and wrist as observed from above, but no accompanying change in pattern of motion (Fig. 4c,f). Differences between speeds are more pronounced in *T. brasiliensis*, apparent in the much more extended wing during the upstroke at low speeds (Fig. 4a,d,h,j). *M. velifer* shows less speed-dependent variation in trajectory of the wrist and digits, wing flexion, sweep angle, and angle of attack than *T. brasiliensis* (Fig. 4). Stroke plane is almost vertical in both *M. velifer* and *T. brasiliensis*, and does not change significantly with speed in either species (see above and Suppl. Table 1), nor does this angle differ significantly between the two species ($p = 0.102$, Fig. 3h; also see Fig. 4b,e; Table 2).

In all, kinematics in *M. velifer* and *T. brasiliensis* are very similar. When specific kinematic parameters are compared within each speed class, using the mixed effect model with Bonferroni correction (Table 2), no significant difference remains at medium speed and only the angle of attack at mid-downstroke ($\alpha_{\text{md}}, p' < 0.001$) and mean angle of attack ($\alpha_{\text{mean}}, p' < 0.001$) differ significantly at high speeds. The main difference between the two species occurs at low speeds, with significant differences in mean angle of attack ($\alpha_{\text{mean}}, p' = 0.04$), body-wingtip distance ($p' < 0.001$) and sweep

angle ($p'=0.018$), which are greater in *T. brasiliensis* than *M. velifer*.

Wake structure

The wakes of *M. velifer*, visualized from the 2D velocity fields and their subsequent 3D reconstructions, were characterized by the vortex structures typically observed in the wakes of flying bats: a tip vortex (V1), a near-body or root vortex (V2), and a distal vortex pair (V3, V4) observed at the end of the upstroke [23, 24, 32-34, 51, 53] (Fig. 5, Suppl. Fig. 2). Wake patterns of individual wing beat cycles showed considerable variation, even at similar speeds, but a general pattern can be discerned within the variation. At low speeds, the wingtip vortex was usually present throughout the wingbeat cycle. At moderate and higher speeds, the tip vortex was often greatly diminished during the upstroke, sometimes to a degree that it was no longer detectable, suggesting that part of the upstroke is aerodynamically passive. The root vortex, shed from wing root at the base of the wing at the body wall, and a distal vortex pair (also known as a “reverse vortex loop”) were detected in some of the trials at all speeds, but frequently fell below the detection threshold of vorticity and swirl. Their occurrence and strength (circulation) diminished as speed increased. Based on the vorticity field, we determined occurrence (O, reported as percentage of all trials within speed group) for the root vortex and distal vortex pair in the three speed categories for both *M. velifer* and *T. brasiliensis* (Table 3). Vortex structure varied with speed in both *M. velifer* and *T. brasiliensis* (Fig. 5, Fig. 6). The wakes of *M. velifer* and *T. brasiliensis* are similar at high speed, where both species are characterized by wakes dominated by a tip vortex that has notable circulation primarily during the downstroke and little vorticity in the upstroke. They are less similar at lower speeds, in which *M. velifer* often lacks a detectable root vortex, and in the 50% of trials in which it is visible, it is always considerably weaker than in *T. brasiliensis* (Fig. 6).

DISCUSSION

Flying animals vary greatly in the architecture of the flight apparatus and their locomotor capabilities. Analyses of wake structure and kinematics can provide insight into the determinants of flight performance that can facilitate comparisons among diverse fliers [20, 24, 54]. Specifically, the nature of the wake vortices reveals details

of aerodynamic force production. Researchers have observed some structural features in the wakes of most bat species studied to date, particularly wingtip, wing root and distal paired vortices, for flight behaviour from hovering to moderately high speeds.

Strong tip vortices are universally present throughout bat downstrokes, confirming their dominant role as a signature of lift generation [23, 24, 31, 33]. In most cases, tip vortices persist through the upstroke although they decline in strength, indicating that the upstroke as well as the downstroke is aerodynamically active [31, 33]. However, in *T. brasiliensis*, at high flight speeds, the tip vortex is greatly diminished or absent for a substantial part of the upstroke, indicating that it is largely aerodynamically passive [24].

Root vortices indicate diminished lift generation over the body relative to the wings; in extreme cases, the body generates no lift, and each wing operates as an independent lifting surface [20, 33, 55, 56]. In this case, root vortices have the same strength as the tip vortices. The distal vortex pair indicates negative lift generation at the distal part of the wing by showing a reversed rotational direction relative to the tip and root vortex pair [51], and it arises at the end of the upstroke, when negative angles of attack are high at the distal part of the wing. Both *T. brasiliensis* and *M. velifer* show wingtip, root, and paired distal vortices to various degrees and depending on flight speeds.

The wake structure is directly related to kinematics and morphology; kinematics might be a direct result of the morphology, but it is difficult to separate these factors. Our detailed analysis shows *M. velifer* and *T. brasiliensis* are similar in kinematics and wake structure at higher speeds, but show notable differences at lower speeds (Fig. 3,4, Table 2). Despite those differences at low speeds, the flight style of these insectivorous aerial hunters looks similar when compared to that of the frugivorous *Cynopterus brachyotis* [32, 33] from the family Pteropodidae (Suppl. Movie 1, previously compared to *T. brasiliensis* [24]). Both insectivores employ an almost vertical stroke plane over a range of flight speeds (Fig. 3, Table 2, Suppl. Table 1). This contrasts with the angled and speed-dependent stroke planes of diverse frugivorous pteropodid bats, distantly related to the focal taxa of this study, who diverged from other bat families more than 55 mya [37, 49]. This effect is not solely

phylogenetic; kinematics of phyllostomid fruit- and nectar-feeding bats *Glossophaga soricina* [57], *Leptonycteris yerbabuena* [52], *Carollia perspicillata* and *Artibeus jamaicensis* (unpublished data) are similar to those of pteropodids [49] and not to the species in this study (see Suppl. Movie 1-4). In particular, they all show relatively tilted stroke planes, especially at low flight speeds, and substantial flexion in the handwing [52, 57].

Previous studies suggest fruit- and nectar-feeding bats shed root vortices over a broad range of flight speeds [23, 33]. Both aerial hunters in this study show only very weak or non-detectable root vortices at high flight speeds. Moreover, while *T. brasiliensis* generates strong root vortices at low speed, *M. velifer* shows little or no vorticity at the wing root at low speed (Table 3, Fig. 5,6). Weak root vortices over a range of speeds, as shown by *M. velifer*, have previously been observed in the pied flycatchers (*Ficedula hypoleuca*) and the blackcaps (*Sylvia atricapilla*) [4, 21].

An ideal wing has an elliptical circulation distribution and generates a uniform downwash [58, 59]. Span efficiency, a measure of deviation from this ideal, has recently been used to quantify differences in flight performance between species [4, 20, 54]. The instrumentation configuration employed in these experiments (varying distance between the animal and the PIV plane, and the relatively small half-span measurement volume) does not allow sufficiently high resolution quantification of span efficiency. Deformation of the wake and the large variation of the wingspan during the stroke cycle can introduce errors in the determination of both lift and span efficiency [19, 20]. However, although quantitative assessment of aerodynamic efficiency was not feasible, qualitative assessment, using the wake structure, was possible. Root vortices have been observed in diverse taxa [21, 24, 31-33, 36, 56, 60, 61]; they indicate that the circulation over the body is less than over the wings, and have been linked to either a broad body disrupting the downwash profile [56] or the petiolation of the wing [61]. While span efficiency is not a direct measure of flight efficiency, because it neglects analysis of parasite and profile drag, it has been shown to be a good indicator of flight cost [20]. Lower span efficiency (due to lower body lift) is understood to result in a lower lift-to-drag ratio and therefore higher mechanical cost of transport [54]. Span efficiency estimates are less compelling as

performance metrics for bodies with very unfavourable lift-to-drag ratios, especially at higher speeds, at which parasite and profile drag increase.

The lack of root vortices at higher speeds in *M. velifer* and *T. brasiliensis* suggests efficient flight in both species and corresponds to the predicted low cost of transport in the migratory *T. brasiliensis* at its ranging speeds. *M. velifer* is similar, however, to *T. brasiliensis* in this respect, despite its different flight ecology, which, based on current records, does not include extensive commuting flight. We suggest that comparisons of flight efficiency at the upper extreme of free-flight speed ranges, exceeding the speeds measured in this study, might be particularly informative.

Strong root vortices appear in *T. brasiliensis* at lower speeds, at which *M. velifer* shows much weaker (lower circulation) and less frequent root vortices. This contrast in wake architecture between the two insectivorous bats suggests a larger difference between body and wing circulation for *T. brasiliensis* than *M. velifer*. This difference might arise from any of a number of mechanisms, including differences in lift generation by the body and/or tail surfaces, differences in body width, or differences in wing loading. Each of these is considered in the following discussion.

Tails play a significant role in lift generation in birds, especially at lower speeds, evidenced by the generation of a distinct tail vortex pair [4, 36]. However, unlike that of birds, the bat tail is connected to the wings via the legs and therefore does not have the potential to be an independent control and lifting surface. Bat species studied to date have little or no tail membrane and bat wakes show no evidence of significant aerodynamic function for the tail [23, 33, 51]. However, both *M. velifer* and *T. brasiliensis* possess substantial tail membranes, and, in common with many insectivorous bats, use tail membranes to capture prey. The ratio of tail to wing area is similar in the two species, (*T. brasiliensis*: $7.3 \pm 0.9\%$; *M. velifer*: $6.6 \pm 0.6\%$), and neither showed evidence of tail vortices at any speed. However, we cannot unequivocally exclude that interspecific differences in tail membrane morphology, such as aspect ratio, could influence the wake structure near the body.

Both species show a low angle of body and tail (see Suppl. Movie 1) at all flight speeds, an observation confirmed when using the foot-body angle as approximation

(Fig. 4a-f). Although this approximation has to be treated with some caution, average foot-body angle over the wingbeat cycle suggests a slightly steeper angle for *M. velifer* (*T. brasiliensis*: $3.2 \pm 5.3^\circ$; *M. velifer*: $9.0 \pm 5.1^\circ$) which would be better for lift generation, and would thus result in weaker root vortices at low speed than observed in *T. brasiliensis*. A second potential explanation for the differences in root vortex structure could be that the body of *T. brasiliensis* is wider than that of *M. velifer*, which may result in a bigger disruption between the wings (body width $13.8 \pm 0.77\%$ of mid-downstroke wingspan in *T. brasiliensis*, $N = 5$; $9.5 \pm 0.9\%$ in *M. velifer*, $N = 4$) (Fig. 2). Lastly, differences in wing loading could contribute to the differences in the root vortex strength at low speed. It has been estimated that wing loading, Q , is almost twice as high for *T. brasiliensis* as *M. velifer* [25]. This parameter can, however, vary substantially depending on the measurement method and current body weight, which fluctuates with many factors. Using the maximum wing area measured in-flight (not including body and tail), our measurements suggest approximately 20% lower wing loading in *M. velifer* than *T. brasiliensis* (11.1 ± 2.1 vs 14.4 ± 2.5 N/m²), primarily due to lower body mass, coupled with larger wing chord (Table 1). Although the wing circulation, Γ , for both species is comparable ($\Gamma \propto Qc$), the coefficient of lift, C_L , which scales with wing loading at a given speed, is significantly lower in *M. velifer*. This reasoning suggests that the induced drag coefficient, C_{Di} , which correlates with the strength of the tip and root vortices, is sharply reduced in *M. velifer* ($C_{Di} \propto C_L^2/AR$). This argument is further supported by the observation that *T. brasiliensis* generally shows higher angles of attack than *M. velifer*, consistent with the generation of a lower coefficient of lift.

Comparing *M. velifer* and *T. brasiliensis* with two aerial hunting birds (the pied flycatcher [4] and the swift [36]) shows a similar relationship between the bat and bird pairs. Both birds are aerial hunters, but like *M. velifer*, the pied flycatcher hunts closer to the ground [62] and has a lower aspect ratio and lower wing loading than the swift [4, 36]. Like *M. velifer*, the pied flycatcher shows rather weak root vortices at both lower and higher speeds (3 ms⁻¹ and 7 ms⁻¹), while swifts have strong root vortices at speeds between 5.7 - 9.9 ms⁻¹. Assuming a correlation between wing loading and root vortices, one might speculate that in swifts, root vortices are

preserved in at higher speeds due to considerably higher wing loading than any of the other species (approx. 26 Nm^{-1}).

Both insectivorous bats show wake structures that are associated with economic flight at higher speeds. This comes as no surprise for *T. brasiliensis* given their extended travel distances. At lower speeds, *M. velifer* seems to have better flight efficiency, indicated by the lack of root vortices, than *T. brasiliensis*. However, the complicated relationship between flight performance, morphology and kinematics makes it impossible to conclusively identify a deterministic role of the parameters we investigated, such as wing loading, aspect ratio, and body width on wake architecture.

Based on the cases in which span efficiency has been used to compare flight performance between species [4, 20, 54], it has been proposed that birds have superior aerodynamic performance to that of bats [54]. This conclusion relies on the fact that the frugivorous bat species investigated (*G. soricina* and *L. yerbabuena*) have lower lift generation associated with the body region than the birds (flycatchers and blackcaps), and as a result, possess relatively low span efficiency. However, the aerial hunting bats in the present study showed weak root vortices at high speeds, indicating the participation of the body in lift generation, and thus suggesting a higher span efficiency, perhaps comparable to the aerial-hunting birds. This wide variation in nature of bat wakes emphasizes the aeromechanical diversity of the order, and consequently, generalisations about bat aerodynamic performance should be made with caution. Further studies that sample a greater diversity of species are needed to elucidate the degree to which the morphologies, kinematics and aerodynamics of birds and bats result from phylogenetic constraints and/or ecological requirements.

ACKNOWLEDGEMENTS

We thank Daniel Riskin, Arnold Song and Rye Waldman for help with experiments, Barbara French and Louise Allen for expertise and help in handling bats, and Anna Wilson for comments on the manuscript. Special thanks to Jorn Cheney, Cosima Schunk and Daniel Riskin for video material. This work was supported by AFOSR and NSF.

ETHICS

All experiments and animal husbandry complied with a protocol approved by the Brown University IACUC and with USDA regulations.

COMPETING INTERESTS

We have no competing interests.

REFERENCES:

- [1] Taylor, G.K., Nudds, R.L. & Thomas, A.L.R. 2003 Flying and swimming animals cruise at a Strouhal number tuned for high power efficiency. *Nature* **425**, 707-711.
- [2] Hedrick, T.L., Cheng, B. & Deng, X. 2009 Wingbeat Time and the Scaling of Passive Rotational Damping in Flapping Flight. *Science* **324**, 252-255.
- [3] Ellington, C.P., van den Berg, C., Willmott, A.P. & Thomas, A.L.R. 1996 Leading-edge vortices in insect flight. *Nature* **384**, 626-630.
- [4] Muijres, F.T., Bowlin, M.S., Johansson, L.C. & Hedenstrom, A. 2012 Vortex wake, downwash distribution, aerodynamic performance and wingbeat kinematics in slow-flying pied flycatchers. *J. R. Soc. Interface* **9**, 292-303.
- [5] Muijres, F.T., Johansson, L.C., Barfield, R., Wolf, M., Spedding, G.R. & Hedenström, A. 2008 Leading-Edge Vortex Improves Lift in Slow-Flying Bats. *Science* **319**, 1250-1253.
- [6] Warrick, D.R., Tobalske, B.W. & Powers, D.R. 2009 Lift production in the hovering hummingbird. *Proceedings of the Royal Society B: Biological Sciences* **276**, 3747-3752.
- [7] Bomphrey, R.J. 2012 Advances in animal flight aerodynamics through flow measurement. *Evolutionary Biology* **39**, 1-11.
- [8] Miller, L.A. & Peskin, C.S. 2009 Flexible clap and fling in tiny insect flight. *J. Exp. Biol.* **212**, 3076-3090.
- [9] Portugal, S.J., Hubel, T.Y., Fritz, J., Heese, S., Trobe, D., Voelkl, B., Hailes, S., Wilson, A.M. & Usherwood, J.R. 2014 Upwash exploitation and downwash avoidance by flap phasing in ibis formation flight. *Nature* **505**, 399-402. (doi:10.1038/nature12939).
- [10] Reynolds, K.V., Thomas, A.L. & Taylor, G.K. 2014 Wing tucks are a response to atmospheric turbulence in the soaring flight of the steppe eagle *Aquila nipalensis*. *J. R. Soc. Interface* **11**. (doi:10.1098/rsif.2014.0645).
- [11] Cheney, J., Konow, N., Middleton, K., Breuer, K., Roberts, T., Giblin, E. & Swartz, S. 2014 Membrane muscle function in the compliant wings of bats. *Bioinsp. Biomim.* **9**, 025007. (doi:10.1088/1748-3182/9/2/025007).
- [12] Laurent, C.M., Palmer, C., Boardman, R.P., Dyke, G. & Cook, R.B. 2014 Nanomechanical properties of bird feather rachises: exploring naturally occurring fibre reinforced laminar composites. *J. R. Soc. Interface* **11**, 20140961.

- [13] Lingham-Soliar, T. 2014 Feather structure, biomechanics and biomimetics: the incredible lightness of being. *Journal of Ornithology* **155**, 323-336.
- [14] Smith, C., Herbert, R., Wootton, R. & Evans, K. 2000 The hind wing of the desert locust (*Schistocerca gregaria* Forskal). II. Mechanical properties and functioning of the membrane. *J. Exp. Biol.* **203**, 2933-2943.
- [15] Vincent, J.F. & Wegst, U.G. 2004 Design and mechanical properties of insect cuticle. *Arthropod. Struct. Dev.* **33**, 187-199.
- [16] Altshuler, D.L., Bahlman, J.W., Dakin, R., Gaede, A.H., Goller, B., Lentink, D., Segre, P.S. & Skandalis, D.A. 2015 The biophysics of bird flight: functional relationships integrate aerodynamics, morphology, kinematics, muscles, and sensors 1. *Can. J. Zool.* **93**, 961-975.
- [17] Dudley, R. 2002 *The biomechanics of insect flight: form, function, evolution*, Princeton University Press.
- [18] Swartz, S. & Konow, N. 2015 Advances in the study of bat flight: the wing and the wind. *Can. J. Zool.* **93**, 977-990.
- [19] Bomphrey, R.J., Henningsson, P., Michaelis, D. & Hollis, D. 2012 Tomographic particle image velocimetry of desert locust wakes: instantaneous volumes combine to reveal hidden vortex elements and rapid wake deformation. *J. R. Soc. Interface* **9**, 3378-3386.
- [20] Henningsson, P. & Bomphrey, R.J. 2013 Span efficiency in hawkmoths. *J. R. Soc. Interface* **10**, 1742-5662 (doi:10.1098/rsif.2013.0099).
- [21] Johansson, L.C. & Hedenström, A. 2009 The vortex wake of blackcaps (*Sylvia atricapilla* L.) measured using high-speed digital particle image velocimetry (DPIV). *J. Exp. Biol.* **212**, 3365-3376.
- [22] Henningsson, P. & Hedenstrom, A. 2011 Aerodynamics of gliding flight in common swifts. *J. Exp. Biol.* **214**, 382-393.
- [23] Muijres, F.T., Johansson, L.C., Winter, Y. & Hedenström, A. 2011 Comparative aerodynamic performance of flapping flight in two bat species using time-resolved wake visualization. *J. R. Soc. Interface* **211**, 2909-2918.
- [24] Hubel, T.Y., Hristov, N.I., Swartz, S.M. & Breuer, K.S. 2012 Changes in kinematics and aerodynamics over a range of speeds in *Tadarida brasiliensis*, the Brazilian free-tailed bat. *J. R. Soc. Interface* **9**, 1120-1130.
- [25] Norberg, U.M. & Rayner, J.M.V. 1987 Ecological morphology and flight in bats (Mammalia; Chiroptera): wing adaptations, flight performance, foraging strategy and echolocation. *Phil. Trans. R. Soc. Lond. B* **316**, 335-427.
- [26] Brewer, M.L. & Hertel, F. 2007 Wing morphology and flight behavior of peleciform seabirds. *J. Morphol.* **268**, 866-877.
- [27] Johansson, F., Söderquist, M. & Bokma, F. 2009 Insect wing shape evolution: independent effects of migratory and mate guarding flight on dragonfly wings. *Biol. J. Linn. Soc.* **97**, 362-372.
- [28] Lockwood, R., Swaddle, J.P. & Rayner, J.M. 1998 Avian wingtip shape reconsidered: wingtip shape indices and morphological adaptations to migration. *J. Avian Biol.*, 273-292.
- [29] Marchetti, K., Price, T. & Richman, A. 1995 Correlates of wing morphology with foraging behaviour and migration distance in the genus *Phylloscopus*. *J. Avian Biol.*, 177-181.
- [30] Muijres, F.T., Spedding, G.R., Winter, Y. & Hedenström, A. 2011 Actuator disk model and span efficiency of flapping flight in bats based on time-resolved PIV measurements. *Exp. Fluids* **51**, 511-525.

- [31] Hedenström, A., Muijres, F., von Busse, R., Johansson, L., Winter, Y. & Spedding, G. 2009 High-speed stereo DPIV measurement of wakes of two bat species flying freely in a wind tunnel. *Exp. Fluids* **46**, 923-932.
- [32] Hubel, T., Hristov, N., Swartz, S.M. & Breuer, K.S. 2009 Time-resolved wake structure and kinematics of bat flight. *Exp. Fluids* **46**, 933-943.
- [33] Hubel, T.Y., Riskin, D.K., Swartz, S.M. & Breuer, K.S. 2010 Wake structure and wing kinematics: the flight of the lesser dog-faced fruit bat, *Cynopterus brachyotis*. *J. Exp. Biol.* **213**, 3427-3440.
- [34] von Busse, R., Waldman, R.M., Swartz, S.M., Voigt, C.C. & Breuer, K.S. 2014 The aerodynamic cost of flight in the short-tailed fruit bat (*Carollia perspicillata*): comparing theory with measurement. *J. R. Soc. Interface* **11**, 20140147.
- [35] Hedenström, A. & Johansson, L.C. 2015 Bat flight: aerodynamics, kinematics and flight morphology. *The Journal of experimental biology* **218**, 653-663.
- [36] Henningsson, P., Muijres, F.T. & Hedenström, A. 2010 Time-resolved vortex wake of a common swift flying over a range of flight speeds. *J. R. Soc. Interface* **8**, 807-816.
- [37] Shi, J.J. & Rabosky, D.L. 2015 Speciation dynamics during the global radiation of extant bats. *Evolution* **69**, 1528-1545.
- [38] Glass, B.P. 1982 Seasonal movements of Mexican freetail bats, *Tadarida brasiliensis mexicana*, banded in the Great Plains. *Southwest. Nat.* **27**, 127-133.
- [39] Barbour, R.W.D., Barbour, W.H.R.W. & Davis, W.H. 1969 *Bats of America*.
- [40] Williams, T.C., Ireland, L.C. & Williams, J.M. 1973 High altitude flights of the free-tailed bat, *Tadarida brasiliensis*, observed with radar. *J. Mammal.* **54**, 807-821.
- [41] Wilkins, K.T. 1989 *Tadarida brasiliensis*. *Mamm. Species* **331**, 1-10.
- [42] Nowak, R.M. 1994 *Walker's bats of the world*, JHU Press.
- [43] Norberg, U.M. 1990 *Vertebrate flight: mechanics, physiology, morphology, ecology and evolution*. Berlin, Springer-Verlag.
- [44] Findley, J.S., Studier, E.H. & Wilson, D.E. 1972 Morphologic properties of bat wings. *J. Mammal.* **53**, 429-444.
- [45] Fitch, J.H., Shump, K.A. & Shump, A.U. 1981 *Myotis velifer*. *Mamm. Species* **149**, 1-5.
- [46] Rayner, J.M. 1991 On the aerodynamics of animal flight in ground effect. *Philosophical Transactions of the Royal Society of London B: Biological Sciences* **334**, 119-128.
- [47] Aldridge, H. 1986 Manoeuvrability and ecological segregation in the little brown (*Myotis lucifugus*) and Yuma (*M. yumanensis*) bats (Chiroptera: Vespertilionidae). *Can. J. Zool.* **64**, 1878-1882.
- [48] Abdel-Aziz, Y. & Karara, H., 1971, Direct linear transformation into object space coordinates in close-range photogrammetry, *Proceedings of the Symposium on Close-Range Photogrammetry* Falls Church, Virginia, U.S.A., 1-18
- [49] Riskin, D.K., Iriarte-Diaz, J., Middleton, K.M., Breuer, K.S. & Swartz, S.M. 2010 The effect of body size on the wing movements of pteropodid bats, with insights into thrust and lift production. *J. Exp. Biol.* **213**, 4110-4122.
- [50] Adrian, R.J., Christensen, K.T. & Liu, Z.C. 2000 Analysis and interpretation of instantaneous turbulent velocity fields. *Exp. Fluids* **29**, 275-290.
- [51] Johansson, L.C., Wolf, M., von Busse, R., Winter, Y., Spedding, G.R. & Hedenström, A. 2008 The near and far wake of Pallas' long tongued bat (*Glossophaga soricina*). *J. Exp. Biol.* **211**, 2909-2918.

- [52] Von Busse, R., Hedenstrom, A., Winter, Y. & Johansson, L.C. 2012 Kinematics and wing shape across flight speed in the bat, *Leptonycteris yerbabuenae*. *Biology Open* **1**, 1226-1238. (doi:10.1242/bio.20122964).
- [53] Hedenström, A., Johansson, L.C., Wolf, M., von Busse, R., Winter, Y. & Spedding, G.R. 2007 Bat flight generates complex aerodynamic tracks. *Science* **316**, 894-897.
- [54] Muijres, F.T., Johansson, L.C., Bowlin, M.S., Winter, Y. & Hedenstrom, A. 2012 Comparing Aerodynamic Efficiency in Birds and Bats Suggests Better Flight Performance in Birds. *PLoS ONE* **7**, e37335. (doi:10.1371/journal.pone.0037335).
- [55] Henningson, P., Spedding, G.R. & Hedenström, A. 2008 Vortex wake and flight kinematics of a swift in cruising flight in a wind tunnel. *J. Exp. Biol.* **211**, 717-730.
- [56] Bomphrey, R.J., Taylor, G.K. & Thomas, A.L. 2009 Smoke visualization of free-flying bumblebees indicates independent leading-edge vortices on each wing pair. *Exp. Fluids* **46**, 811-821.
- [57] Wolf, M., Johansson, L.C., von Busse, R., Winter, Y. & Hedenstrom, A. 2010 Kinematics of flight and the relationship to the vortex wake of a Pallas' long tongued bat (*Glossophaga soricina*). *J. Exp. Biol.* **213**, 2142-2153.
- [58] Spedding, G. & McArthur, J. 2010 Span efficiencies of wings at low Reynolds numbers. *Journal of Aircraft* **47**, 120-128.
- [59] Anderson, J.D. 2001 *Fundamentals of aerodynamics*. 3rd ed, Tata McGraw-Hill Education.
- [60] Henningson, P., Michaelis, D., Nakata, T., Schanz, D., Geisler, R., Schröder, A. & Bomphrey, R.J. 2015 The complex aerodynamic footprint of desert locusts revealed by large-volume tomographic particle image velocimetry. *J. R. Soc. Interface* **12**, 20150119.
- [61] Brodsky, A. 1991 Vortex formation in the tethered flight of the peacock butterfly *Inachis io* L. (Lepidoptera, Nymphalidae) and some aspects of insect flight evolution. *J. Exp. Biol.* **161**, 77-95.
- [62] Davies, N.B. 1977 Prey selection and the search strategy of the spotted flycatcher (*Muscicapa striata*): a field study on optimal foraging. *Anim. Behav.* **25**, 1016-1033.

FIGURES

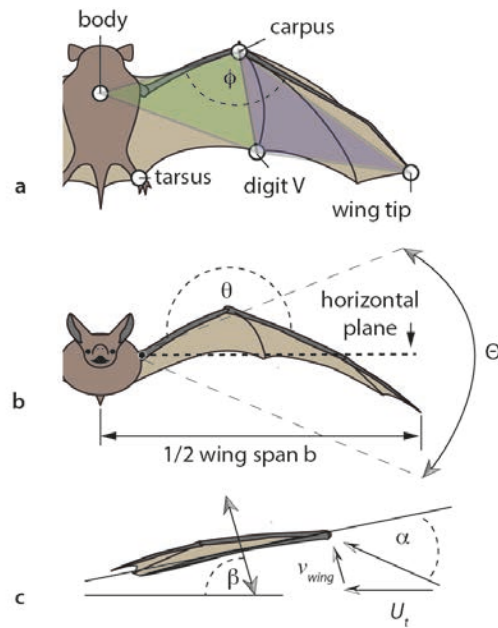


Figure 1: Anatomical features, marker positions and kinematic parameters. (a) dorsal view; ϕ , sweep angle, proximal plane is shaded green, distal plane is shaded blue, (b) front view; θ , flex angle; Θ , amplitude angle (c) simplified side view (wing only); α = angle of attack, β = stroke plane angle, U_t = total forward speed, v_{wing} = wing velocity at wrist.

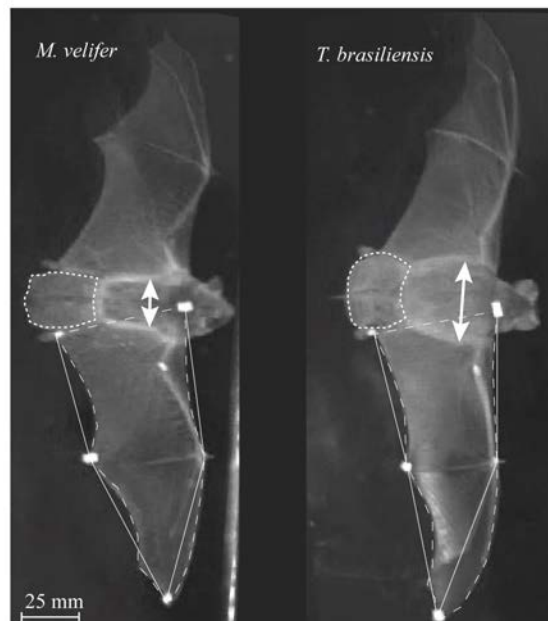


Figure 2: Dorsal view of *M. velifer* and *T. brasiliensis* at low speed, mid-downstroke. Tail area (fine dashed line); mid-body width (arrows); 5-point wing area (solid line) and contour area (dashed line).

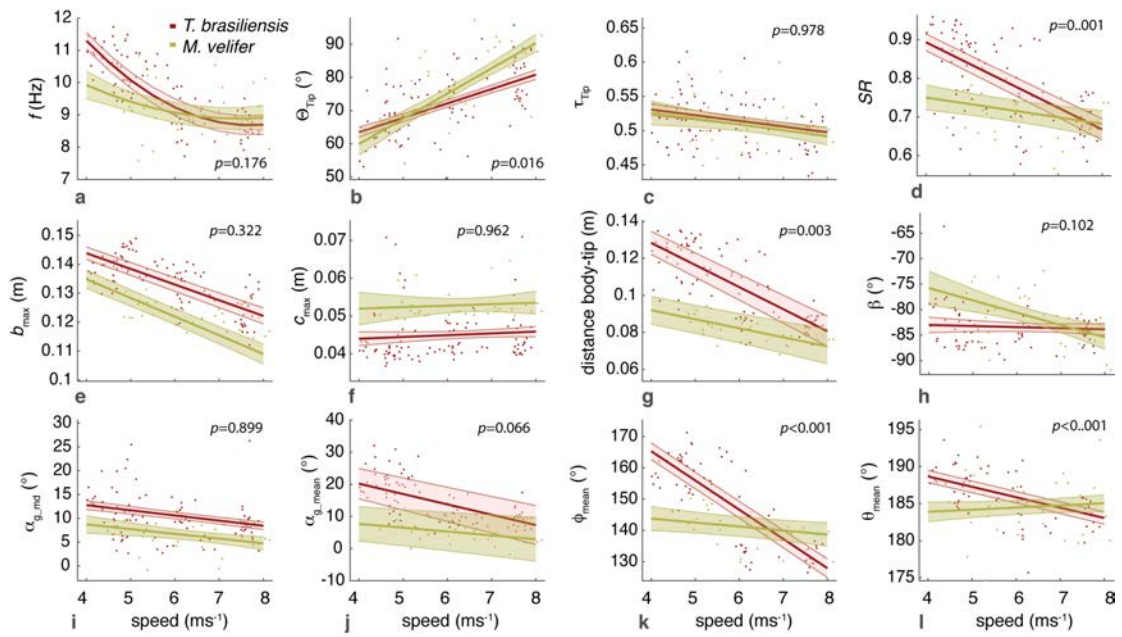


Figure 3: Variation in kinematic parameters across flight speed for *M. velifer* and *T. brasiliensis*. (a) frequency, (b) amplitude, (c) downstroke ratio, (d) span ratio, (e) maximum half wingspan, (f) maximum chord, (g) minimum body wing tip distance, (h) stroke plane angle, (i) angle of attack mid downstroke, (j) mean angle of attack, (k) mean sweep angle, (l) mean flexion angle. All graphs represent the best fit of the mixed effect model for each species; the shaded areas represent the standard error. p -values lower than 0.05 indicate significant difference in slope between species.

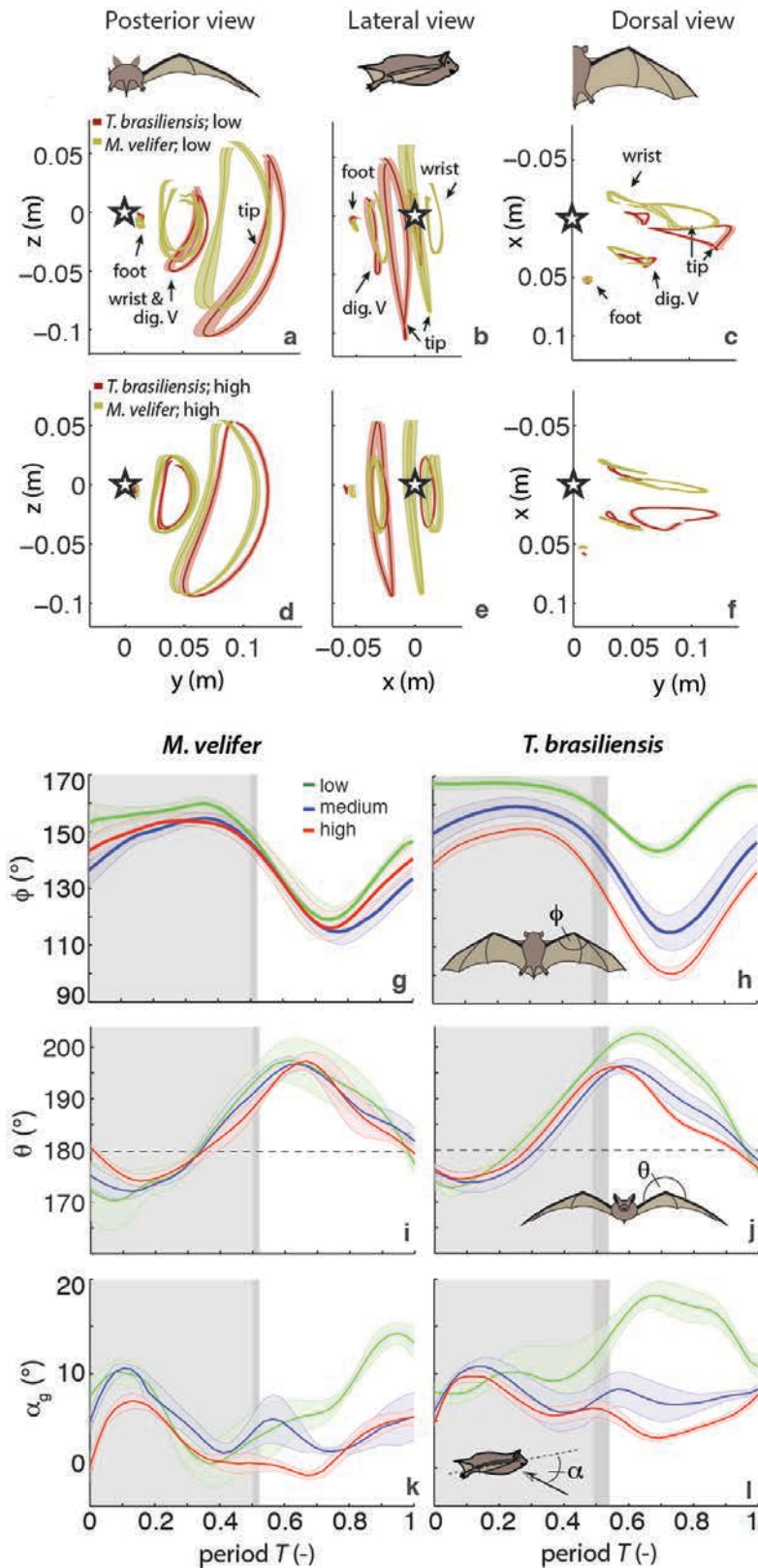


Figure 4: (a – f): Average trajectory of the wingtip, wrist, tip of the digit V (dig. V), and ankle in body-referenced coordinate system for *M. velifer* (green) and *T. brasiliensis* (brown) in two different speed groups. Star indicates body marker position in bat-centred coordinate system. For graphic comparison speeds were grouped in low,

medium and high speeds, trajectories based on the mean of all individual means in these groups, shaded intervals indicate standard error between individual means. Trajectories displayed at low (a – c) and high (d – f) speeds (medium speed not displayed). (i – l): Speed-dependent wrist kinematics *M. velifer* and *T. brasiliensis* at low, medium and high speeds; downstroke indicated by shading (downstroke shorter at higher speeds, darker shading indicates period of variation). (g, h) Wrist sweep angle: ϕ . (i, j) Wrist flexion angle: θ , dashed line indicates no flexion between proximal and distal wing or ‘flat plate’ condition. (k, l) Angle of attack based on armwing or proximal plane.

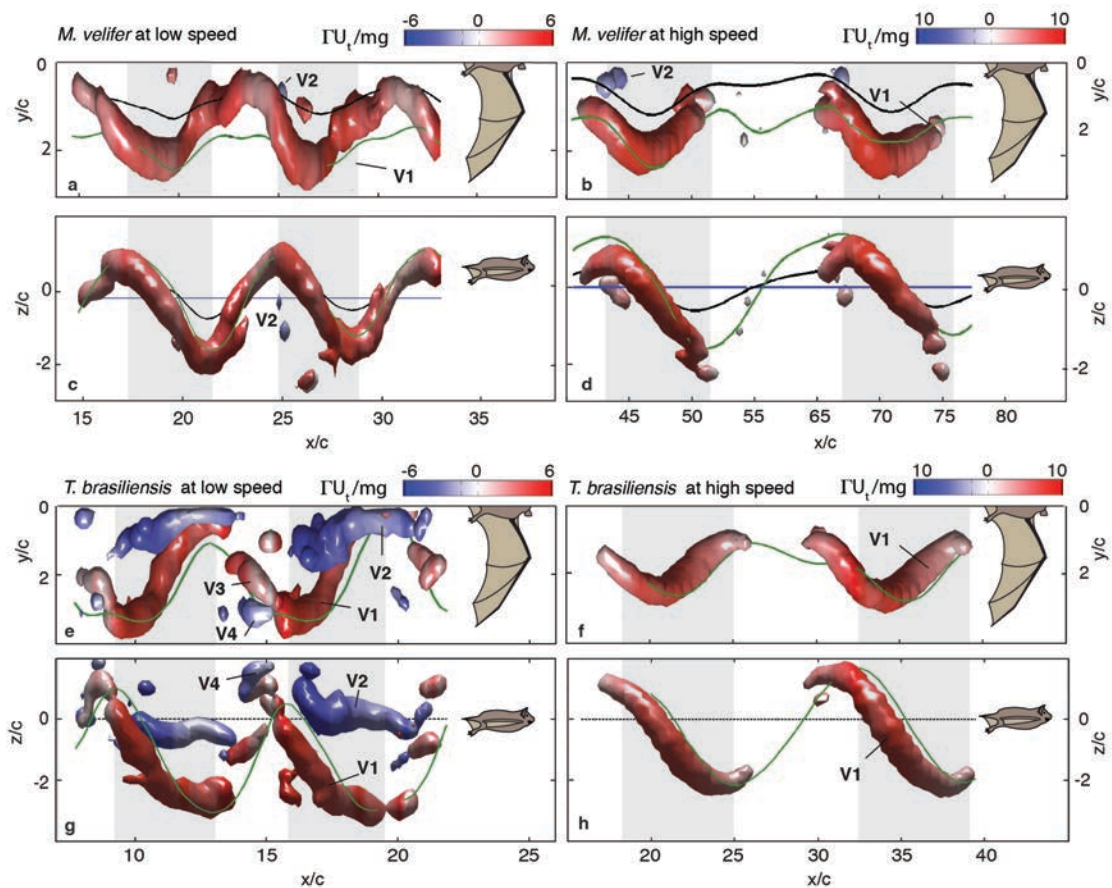


Figure 5: Wake reconstruction for *M. velifer* and *T. brasiliensis* at low and high speed. (a-d) *M. velifer*, (a,b) dorsal view and (c,d) side view at (a,c) low ($U_t = 4.8 \text{ ms}^{-1}$) and (b,d) high speed ($U_t = 8.1 \text{ ms}^{-1}$); (e-h) *T. brasiliensis*, (e,f) dorsal view and (g,h) side view at (e,g) low ($U_t = 5.1 \text{ ms}^{-1}$) and (f,h) high speed ($U_t = 7.0 \text{ ms}^{-1}$). Isosurfaces of transverse swirl are based on 2D PIV; path of right wingtip: green line, path of right wrist: black line, path of body: blue line. Vortices are coloured based on circulation and rotational direction, with counter-clockwise rotating vortices positive (red); tip vortex: V1, root vortex: V2, distal vortex pair: V3 and V4, distance travelled in flow stream direction in chord lengths: x/c , distance perpendicular to midline in chord lengths: y/c .

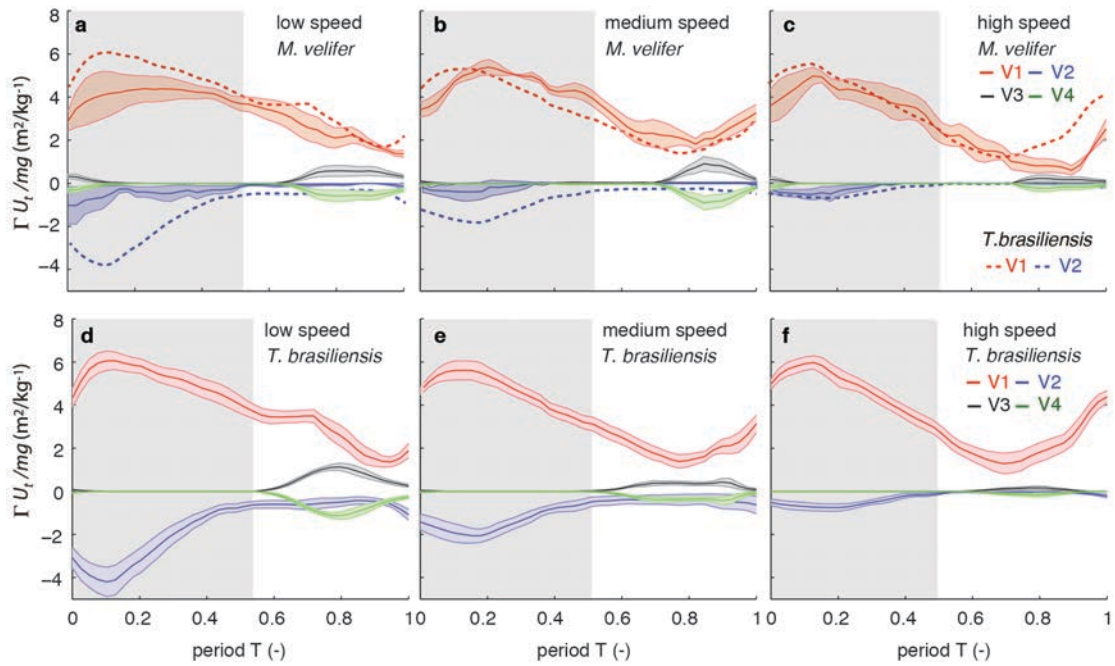


Figure 6: Average circulation for each vortex (V1–V4) normalised by speed and body weight (tip vortex: V1, root vortex: V2, distal vortex pair: V3 and V4) for different speed categories. (a-c) *M. velifer*, (d-f) *T. brasiliensis* at (a,d) low, (b,e) medium and (c,f) high speeds. Dashed lines in a-c show normalised circulations for tip (V1) and root (V2) vortices in *T. brasiliensis*. Shaded intervals: Mean \pm s.e. of individual means, grey shading denotes downstroke.

TABLES

Table 1: Morphology of study subjects and number of trials analysed for each individual. Note: body width and tail area were from frames of high speed video at time of maximum wing extension (one per individual). All other means (\pm S.D.) were extracted from flights at low speed from of a total of 25 wingbeat cycles in *M. velifer* and 57 in *T. brasiliensis*.

ID	sex	half span b_{max} (m)	chord c_{max} (m)	mass m (g)	one wing area S (cm ²)	total aspect ratio AR (-)	wing loading Q (N/m ²)	mid body width (m)	total tail area (cm ²)	number of trials
<i>M. velifer</i>										
M I	female	0.124 \pm 0.004	0.051 \pm 0.002	9.16 \pm 0.3	41.6 \pm 4.1	7.3 \pm 0.5	12.8 \pm 1.3	0.028	5.2	10
M II	female	0.132 \pm 0.004	0.054 \pm 0.006	11.9 \pm 0.5	40.7 \pm 5.5	8.6 \pm 0.2	13.0 \pm 1.0	0.028	4.9	8
M III	female	0.130 \pm 0.002	0.055 \pm 0.004	9.65 \pm 0.4	43.2 \pm 4.4	7.8 \pm 0.7	9.3 \pm 1.0	0.026	6.0	6
M IV	male	0.123 \pm 0.004	0.051 \pm 0.001	9.73 \pm 0.5	44.3 \pm 3.9	6.8 \pm 0.5	9.3 \pm 1.5	0.032	6.3	10
mean	-	0.127 \pm 0.004	0.052 \pm 0.002	10.12 \pm 0.6	42.4 \pm 1.6	7.6 \pm 0.3	11.1 \pm 2.1	0.028	5.6	
<i>T. brasiliensis</i>										
T I	female	0.138 \pm 0.003	0.047 \pm 0.023	11.8 \pm 0.4	37.5 \pm 5.6	10.2 \pm 0.5	14.1 \pm 2.3	0.039	5.9	20
T II	female	0.139 \pm 0.003	0.043 \pm 0.005	13.2 \pm 0.4	40.6 \pm 2.4	9.6 \pm 0.8	15.2 \pm 1.0	0.036	6.1	20
T III	male	0.138 \pm 0.004	0.047 \pm 0.022	11.0 \pm 0.4	37.0 \pm 3.5	10.4 \pm 0.7	13.8 \pm 1.5	0.040	5.7	19
T IV	male	0.147 \pm 0.004	0.045 \pm 0.006	12.4 \pm 0.6	34.6 \pm 9.5	12.5 \pm 0.4	17.8 \pm 8.1	0.041	5.3	20
T V	male	0.147 \pm 0.004	0.045 \pm 0.009	10.5 \pm 0.4	43.6 \pm 2.0	10.0 \pm 0.7	10.7 \pm 1.0	0.040	5.0	20
mean	-	0.142 \pm 0.005	0.045 \pm 0.002	11.8 \pm 1.1	38.6 \pm 3.5	10.5 \pm 0.3	14.4 \pm 2.5	0.039	5.6	

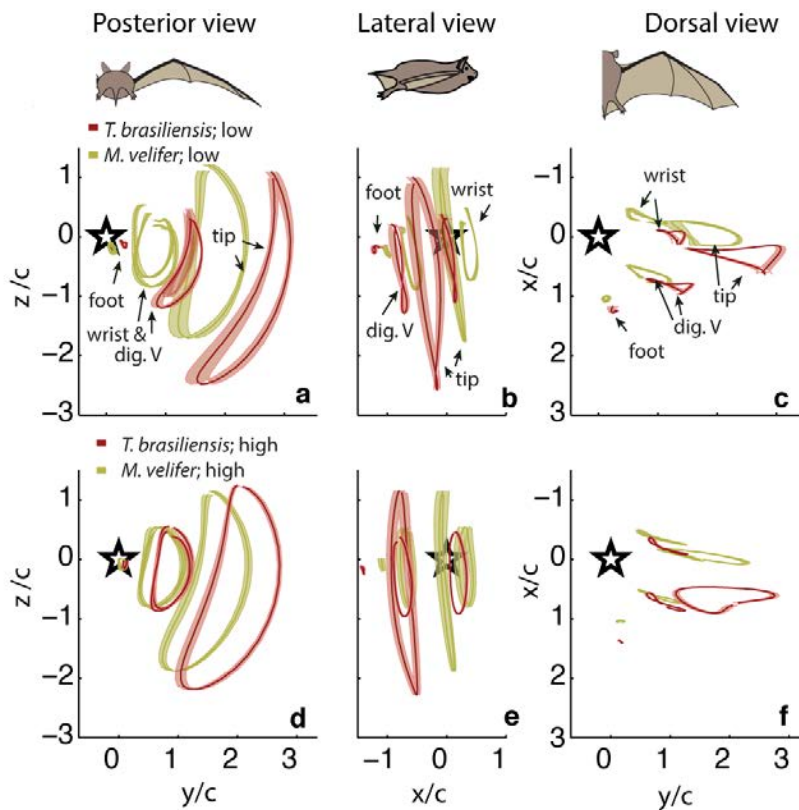
Table 2: Kinematics in *Myotis velifer* and *Tadarida brasiliensis* for three flight speed categories. Means, p - and p' corrected p -values (using sequential Bonferroni), degrees of freedom and t -values.

	<i>M. velifer</i>	<i>T. brasiliensis</i>	parameter estimates			
	Mean \pm s.e.	Mean \pm s.e.	p'	p	df	t
$U_i < 5.5\text{m/s}$						
Wingbeat frequency, f (Hz)	9.30 \pm 0.38	10.48 \pm 0.32	0.28	0.068	4.81	2.34
Wingbeat amplitude, Θ_{tip} ($^\circ$)	66.11 \pm 3.19	66.19 \pm 2.0	1	0.983	9.91	0.02
Downstroke ratio, τ (-)	0.51 \pm 0.011	0.52 \pm 0.007	1	0.621	7.90	0.51
Span ratio, SR (-)	0.86 \pm 0.02	0.74 \pm 0.30	0.077	0.011	8.29	3.28
Minimum distance body – wing tip, d_{min} (m)	0.09 \pm 0.004	0.12 \pm 0.003	<0.001	<0.001	10.13	6.52
Stroke plane angle, β ($^\circ$)	-80.97 \pm 1.97	-83.54 \pm 1.49	1	0.341	5.64	-1.04
Downstroke angle of attack, α_{md} ($^\circ$)	6.81 \pm 1.97	12.38 \pm 1.21	0.324	0.054	-1.46	11.27
Mean angle of attack, α_{mean} ($^\circ$)	5.97 \pm 2.49	18.95 \pm 2.01	0.040	0.005	7.07	4.06
Sweep angle, ϕ ($^\circ$)	147.10 \pm 2.21	159.79 \pm 1.47	0.018	0.002	7.05	4.78
Flexion angle, θ ($^\circ$)	184.62 \pm 1.27	188.20 \pm 0.81	0.324	0.056	5.85	2.38
$5.5\text{m/s} < U_i < 7.0\text{m/s}$						
Wingbeat frequency, f (Hz)	8.91 \pm 0.25	9.06 \pm 0.18	1	0.629	9.89	0.50
Wingbeat amplitude, Θ_{tip} ($^\circ$)	78.06 \pm 3.12	73.42 \pm 1.80	1	0.204	51.24	-1.29
Downstroke ratio, τ (-)	0.51 \pm 0.016	0.52 \pm 0.01	1	0.646	9.95	0.47
Span ratio, SR (-)	0.81 \pm 0.04	0.69 \pm 0.03	1	0.433	8.01	0.83
Minimum distance body – wing tip, d_{min} (m)	0.08 \pm 0.006	0.10 \pm 0.005	0.390	0.056	8.04	2.23
Stroke plane angle, β ($^\circ$)	-79.10 \pm 1.67	-85.37 \pm 1.43	0.234	0.029	5.95	-2.86
Downstroke angle of attack, α_{md} ($^\circ$)	5.47 \pm 1.31	10.80 \pm 1.093	0.14	0.014	1.41	9.27
Mean angle of attack, α_{mean} ($^\circ$)	5.47 \pm 1.31	10.81 \pm 1.09	0.140	0.014	8.10	3.12
Sweep angle, ϕ ($^\circ$)	137.05 \pm 5.04	143.01 \pm 4.32	1	0.397	7.52	0.90
Flexion angle, θ ($^\circ$)	183.87 \pm 1.70	184.36 \pm 1.46	1	0.833	7.25	0.22
$U_i > 7.5\text{m/s}$						
Wingbeat frequency, f (Hz)	8.91 \pm 0.32	8.74 \pm 0.24	1	0.690	5.91	-0.42
Wingbeat amplitude, Θ_{tip} ($^\circ$)	87.04 \pm 2.38	80.25 \pm 1.43	0.252	0.036	9.33	-2.44
Downstroke ratio, τ (-)	0.49 \pm 0.011	0.49 \pm 0.007	1	0.697	5.01	0.41
Span ratio, SR (-)	0.68 \pm 0.03	0.69 \pm 0.02	1	0.855	6.29	-0.19
Minimum distance body – wing tip, d_{min} (m)	0.07 \pm 0.003	0.08 \pm 0.002	0.192	0.024	5.67	3.04
Stroke plane angle, β ($^\circ$)	-85.6 \pm 3.85	-82.68 \pm 2.18	1	0.496	25.33	0.69
Downstroke angle of attack, α_{md} ($^\circ$)	2.36 \pm 0.79	9.26 \pm 0.53	<0.001	<0.001	4.70	9.11
Mean angle of attack, α_{mean} ($^\circ$)	2.34 \pm 0.91	8.58 \pm 0.60	<0.001	<0.001	8.13	5.68
Sweep angle, ϕ ($^\circ$)	142.27 \pm 4.76	128.92 \pm 3.36	0.402	0.067	5.41	-2.29
Flexion angle, θ ($^\circ$)	184.37 \pm 1.27	183.44 \pm 0.89	1	0.573	5.79	-0.60

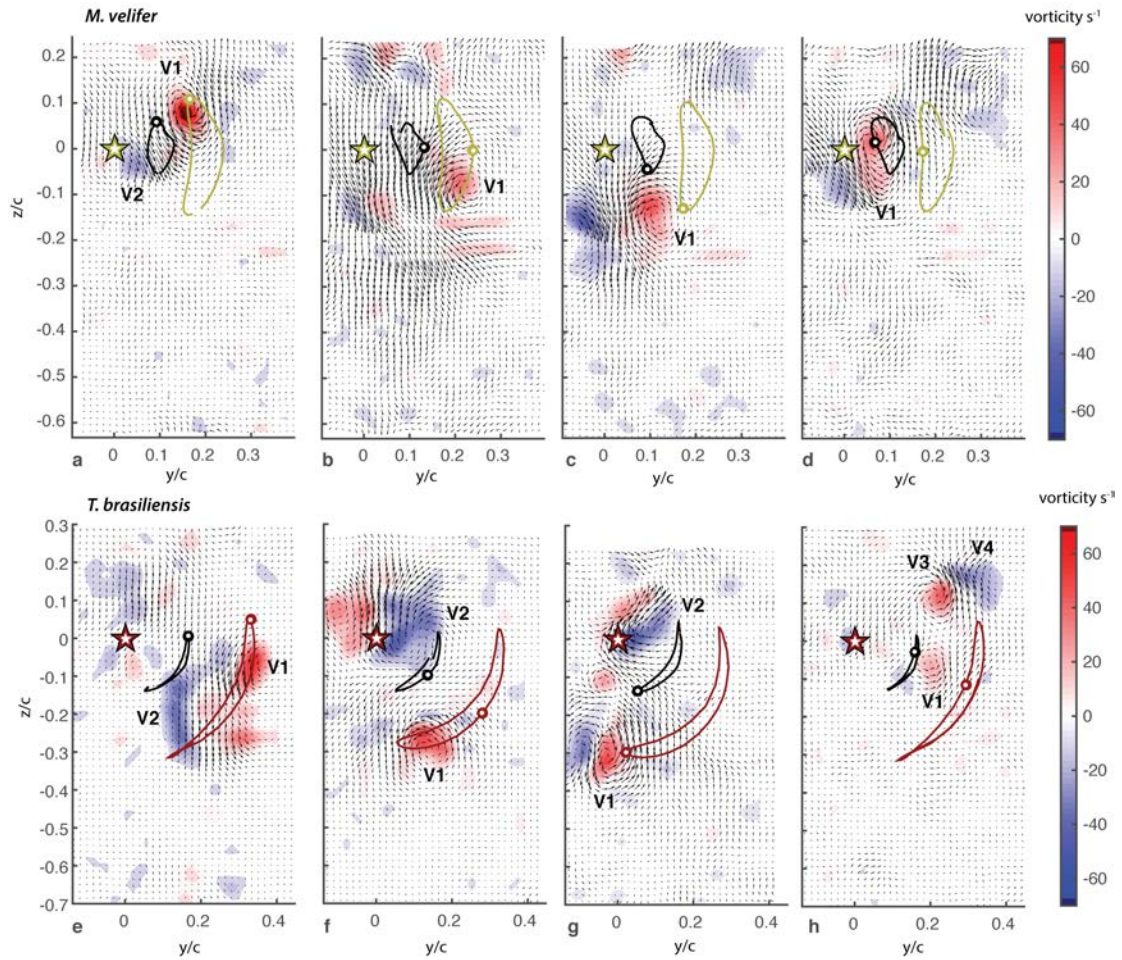
Table 3: Percentage occurrence, O , of root (V2) and distal vortex pair (V3/V4) in relation to species and speed category, based on manual assessment of vorticity fields with a noise reduction threshold of $+ -5\text{ s}^{-1}$ vorticity.

	<i>T. brasiliensis</i>		<i>M. velifer</i>	
	root V2	distal V3	root V2	distal V3
$U_i < 5.5\text{m/s}$	100%	96%	50%	69%
$5.5\text{m/s} < U_i < 7.0\text{m/s}$	93%	83%	18%	70%
$U_i > 7.0\text{m/s}$	76%	15%	20%	27%

SUPPLEMENTARY MATERIAL



Suppl. Fig. 1: a – f: Average trajectory of the wingtip, wrist, tip of digit V (dig. V), and ankle in body-referenced coordinate system, normalized by wing chord for *M. velifer* (green) and *T. brasiliensis* (brown). Star indicates body marker position. For graphic comparison trials were grouped in low, medium and high speeds. Trajectories displayed from low (a – c) and high (d – f) speeds (medium speed not displayed).



Suppl. Fig. 2: Vector velocity fields and streamwise velocity for and *M. velifer* (a-d, at speed 4.81 ms⁻¹) *T. brasiliensis* (e-l, at speed 5.1 ms⁻¹). Mid upstroke (a, e), upper reversal point (b, f), mid downstroke (c, g), lower reversal point (d, h). Star: position of midline trunk marker, wrist trajectory: black line. wingtip trajectory: green line, location of marker at point of cycle depicted in image indicated by open circle (wrist = black, wingtip = green). V1: tip vortex, V2: root vortex, V3 and V4: distal vortex pair.

Suppl. Table 1: Change in kinematics with flight speed in (a) *M. velifer* and (b) *T. brasiliensis*. p' -values: p -values corrected using sequential Bonferroni. (N = 5 individuals; n = 71 wingbeat cycles). Grey arrows indicate significance for only uncorrected p -values. Linear mixed effect model.

<i>M. velifer</i>	increase/ decrease w. speed	p'	p	df	t	lower bound	upper bound
Wingbeat frequency, f (Hz)	↓	0.098	0.014	26.7	-2.64	-0.440	-0.055
Wingbeat amplitude, Θ_{tip} (°)	↑	<0.001	<0.001	33.4	4.81	4.168	10.282
Downstroke ratio, τ (-)	–	0.895	0.21	42.5	-1.27	-0.029	0.007
Span ratio, SR (-)	–	0.895	0.179	32.9	-1.37	-0.037	0.007
Maximum half span, b_{max} (m)	↓	0.020	0.002	34.9	-3.43	-0.010	-0.002
Maximum wing chord, c_{max} (m)	–	1.000	0.921	39.2	0.1	-0.013	0.001
Minimum distance body – wing tip, d_{min} (m)	↓	0.040	0.005	34.8	-3.03	-0.008	-0.002
Stroke plane angle, β (°)	–	0.678	0.113	30.3	-1.63	-2.106	0.234
Downstroke angle of attack, α_{md} (°)	–	1.000	0.476	35.9	-0.72	-2.701	1.286
Mean angle of attack, α_{mean} (°)	↓	0.027	0.003	37.4	-3.22	-2.000	-0.456
Sweep angle, ϕ (°)	–	1.000	0.58	32.6	-0.56	-4.511	2.566
Flexion angle, θ (°)	–	1.000	0.976	33.5	0.03	-1.453	1.497

<i>T. brasiliensis</i>	increase/ decrease w. speed	p'	p	df	t	lower bound	upper bound
Wingbeat frequency, f (Hz)	↓	0.001	<.001	101.1	-12.1	-0.5607	-0.4031
Wingbeat amplitude, Θ_{tip} (°)	↑	0.002	<.001	99.9	8.2	3.2766	5.3673
Downstroke ratio, τ (-)	↓	0.004	0.001	118.6	-3.3	-0.013	-0.0032
Span ratio, SR (-)	↓	0.004	<.001	97.4	-11.6	-0.0638	-0.0452
Maximum half span, b_{max} (m)	↓	0.005	<.001	106.5	-16.1	-0.0059	-0.0046
Maximum wing chord, c_{max} (m)	–	0.956	0.478	127.4	0.7	-0.001	0.0021
Minimum distance body – wing tip, d_{min} (m)	↓	0.005	<.001	102.1	-15.8	-0.0125	-0.0097
Stroke plane angle, β (°)	–	0.956	0.844	63.1	-0.2	-1.4602	1.1968
Downstroke angle of attack, α_{md} (°)	↓	0.005	<.001	58.3	-3.7	-1.5949	-0.4692
Mean angle of attack, α_{mean} (°)	↓	0.005	<.001	86.1	-10.9	-3.4838	-2.4056
Sweep angle, ϕ (°)	↓	0.005	<.001	87.9	-20.2	-10.2434	-8.4066
Flexion angle, θ (°)	↓	0.005	<.001	86.5	-8	-1.6956	-1.0155